ADVANCED FUNCTIONAL MATERIALS
www.afm-journal.de

A Hydrogel Platform that Incorporates Laminin Isoforms for Efficient Presentation of Growth Factors – Neural Growth and Osteogenesis

*Oana Dobre, Mariana A. G. Oliva, Giuseppe Ciccone, Sara Trujillo, Aleixandre Rodrigo-Navarro, Douglas Cormac Venters, Virginia Llopis-Hernandez, Massimo Vassalli, Cristina Gonzalez-Garcia, Matthew J. Dalby, and Manuel Salmeron-Sanchez**

Laminins (LMs) are important structural proteins of the extracellular matrix (ECM). The abundance of every LM isoform is tissue-dependent, suggesting that LM has tissue-specific roles. LM binds growth factors (GFs), which are powerful cytokines widely used in tissue engineering due to their ability to control stem cell differentiation. Currently, the most commonly used ECM mimetic material in vitro is Matrigel, a matrix of undefined composition containing LM and various GFs, but subjected to batch variability and lacking control of physicochemical properties. Inspired by Matrigel, a new and completely defined hydrogel platform based on hybrid LM-poly(ethylene glycol) (PEG) hydrogels with controllable stiffness (1–25 kPa) and degradability is proposed. Different LM isoforms are used to bind and efficiently display GFs (here, bone morphogenetic protein (BMP-2) and beta-nerve growth factor (β-NGF)), enabling their solid-phase presentation at ultralow doses to specifically target a range of tissues. The potential of this platform to trigger stem cell differentiation toward osteogenic lineages and stimulate neural cells growth in 3D, is demonstrated. These hydrogels enable 3D, synthetic, defined composition, and reproducible cell culture microenvironments reflecting the complexity of the native ECM, where GFs in combination with LM isoforms yield the full diversity of cellular processes.

1. Introduction

The ECM forms the niche for tissue residing cells. It is made of a myriad of components including water, polysaccharides, and structural proteins such as LM and fibronectin (FN) that also provide functionality.[1] These two proteins, in particular, play an important role in ECM architecture, cell-adhesion, and binding of numerous molecules, thus influencing cell behavior. They are also involved in matrix remodeling and, therefore, tissue homeostasis. Their important contribution to ECM structure and function has inspired rigorous research efforts focused on recreating these properties in vitro.

Currently, the most commonly used ECM mimetic material is Matrigel, an undefined mix of proteins and GFs derived from Engelbreth–Holm–Swarm mouse sarcoma cells that provide excellent biological functionality.[2] However, batch-to-batch variation, suboptimal mechanical properties, and undefined composition of animal origin make it difficult to determine the exact signals that promote cell function and make it unsuitable for translation to clinic. There have been many unsuccessful attempts to produce an alternative synthetic, defined, culture system that recapitulates the properties of the natural ECM and therefore Matrigel is still widely used for in vitro 3D cell culture.[3] To reproduce the ECM properties in a synthetic system, it is key to incorporate structural proteins such as LM and FN, combined with GFs that play an essential role in many cellular processes.[4] That the ECM acts as a GF reservoir[5] and the GF contribution to cell adhesion and function is almost totally overlooked in synthetic gel culture systems where adhesion peptides remain a focus and suboptimal performance, remains a challenge.

LMs are multimeric glycoproteins, formed of three chains α, β, and γ, and located mainly in the basement membrane (BM).[6] They have an important role in cell differentiation, proliferation, and migration.[7,8] There are sixteen isoforms of LM with tissue-dependent distribution.[6] These include LM332, predominantly found in epithelial, bone, and vascular tissues;[9,10] LM411 and LM111 in the central and peripheral nervous system (CNS and PNS);[11,12] as well as LM221 and LM521 that are mostly expressed in muscle[13,14] and liver,[15] respectively. Furthermore, as well as having tissue-dependent isoforms, different LMs have

Dr. O. Dobre, M. A. G. Oliva, G. Ciccone, Dr. S. Trujillo, Dr. A. Rodrigo-Navarro, Dr. D. C. Venters, V. Llopis-Hernandez, Dr. M. Vassalli, Dr. C. Gonzalez-Garcia, Prof. M. J. Dalby, Prof. M. Salmeron-Sanchez
Centre for the Cellular Microenvironment
University of Glasgow
Glasgow G12 8LT, UK
E-mail: Manuel.Salmeron-Sanchez@glasgow.ac.uk

The ORCID identification number(s) for the author(s) of this article can be found under https://doi.org/10.1002/adfm.202010225.

DOI: 10.1002/adfm.202010225

affinity for different GFs, making them a promising tool in the repair and regeneration of a variety of tissues.[4] Alternative mRNA splicing of LMs produces different isoforms whose abundance is tissue-dependent and have the ability to bind different GFs, making them a more versatile candidate than FN, that only has two different isoforms.[16]

GFs are potent, small cytokines capable of inducing cell differentiation and tissue development. These molecules are widely used in basic and translational research. However, their short half-life, high diffusion coefficient, and cost makes their use in clinic challenging.[17,18] Currently, clinical administration of these molecules involves the use of high doses that have undesired, systemic side effects such as ectopic bone formation and the development of malignant neoplasms.[19] Several strategies for GF delivery have been explored in recent years,[17,20] including their presentation covalently bound to biomaterials,[21,22] and non-covalently bound to peptides that contain domains with affinity for GFs.[23–25]

For example, binding of BMP-2, vascular endothelial growth factor A (VEGF-A), platelet-derived growth factor (PDGF-AB), and insulin-like growth factor 1 (IGF-1) to fibrin matrices.[26–30] Solid-phase presentation of GFs that are non-covalently bound to biomaterials involve the use of peptides that contain domains with affinity for GFs.[23–25]

Another strategy has exploited the affinity of GFs to certain protein sequences, for example, the heparin binding domain in FN ($III_{12\text{-}14}$) or the α chain of LM, to produce fibrin hydrogels combined with these sequences.[31] For example, the LM-derived peptide LAMA33043–3067 was incorporated into fibrin gels and loaded with VEGF-A165 and PDGF-BB to improve skin wound healing of full-thickness.[9] Further, the affinity of VEGF-A and PDGF-BB to the α chain of LM was increased by coupling them to a syndecan-derived peptide (RKRLQVQLSIRT).[32]

Here, we present an approach that makes use of full-length LMs, using well-defined LM isoforms that bind GFs and target specific tissues, a strategy not considered in the literature so far.[9,33–35] For example, hydrogels functionalized with full-length LM111 take advantage of its multiple bioactive domains that bind components of the basal membrane such as nidogen, perlecan, agrin, and collagen IV to enhance nervous tissue regeneration (neurite growth and neural stem cell (NSC) differentiation).[33,36–40] However, there are no studies that exploit the affinity of different GFs to various LM isoforms and their involvement in the organisation of different tissues. Moreover, LM may possess other domains that play a relevant role in the in vivo physiology of the cells, which cannot be mimicked in a short synthetic peptide and will still be functional when using the full-length protein. Furthermore, using full-length ECM proteins contributes to a better recapitulation of the ECM microenvironment and a stronger biological effect than with the use of shorter peptides.[41]

In this work, we present a strategy to develop LM/PEG-based hydrogels that enhance the bioactivity and stability of GFs using selected LM isoforms with specific affinity for GFs. This system closely mimics the native tissue environment both bio-chemically and mechanically. Its stiffness can be tuned to resemble a variety of tissues allowing a broad range of applications. We report the controlled, solid-phase presentation of physiological doses of GFs (here BMP-2 and β-NGF) bound to different LM isoforms. The developed platform can outperform current approaches to deliver tissue-specific GFs, promoting bone and nervous tissue regeneration.

2. Results and Discussion

2.1. 3D Hybrid Laminin Hydrogels with Controlled Degradability and Mechanical Properties

Different LM isoforms were incorporated into a synthetic PEG polymeric network using UV-triggered photo-polymerisation (**Figure 1A**,B,C).[34,35] Human LM isoforms 111, 521, 411, and 332 were first PEGylated with a PEG-acrylate-succinimidyl (PEG-AC-SCM) via a *N*-hydroxysuccinimide (NHS) ester reaction with the primary amines of the protein, forming a stable, covalent amide bond at pH 8.3 and releasing the NHS group (Figure 1C).[34,35] The degree of PEGylation for different LM:AC ratios was measured by tracking the reduction in primary amines after the reaction using a 2,4,6-trinitrobenzene sulfonic acid (TNBSA) assay, which indicated an increase in the LM degree of modification as the LM:AC ratio increased (Figure S1A, Supporting Information). Then, the bioactivity and cell adhesion to LM PEGylated at different ratios (10, 25, and 500 molecules of PEG-AC-SCM per molecule of LM, denoted as 1:10, 1:25, and 1:500 throughout the paper), was tested using C2C12 cells. LM PEGylated at a 1:25 ratio showed a similar adhesion and formation of actin filaments compared to native LM and better than any other LM PEGylation ratios (Figure S1B, Supporting Information). This demonstrates that PEGylation at 1:25 does not alter LM bioactivity.[34,37]

3D LM/PEG hydrogels were produced by mixing PEGylated LM (1:25) with a four-arm acrylate PEG and crosslinkers (either protease-degradable GCRD**VPM**SMRGGDRCG peptide (VPM) or PEG-dithiol (PEG-2SH)) (Figure 1B,C). LM distribution within the LM/PEG hydrogels was evaluated using immunofluorescence, showing a homogeneous distribution of the protein, whereas PEG-only gels did not show any staining (Figure 1D and Figure S2, Supporting Information). An image of the LM/PEG hydrogel after polymerization and hydrogel network structure taken using scanning electronic microscopy (SEM) is shown in Figure 1E. Then, the swelling properties of the gels were assessed over 28 days. After 7 days, the swelling ratio reached a plateau that was maintained at least until day 28 (Figure 1F and Figure S4B, Supporting Information) revealing the stability of the crosslinking process.

Cells are known to remodel their environment by the secretion of matrix metalloproteases (MMPs).[42,43] Recently, cells have been shown to secrete ECM proteins pericellularly and/or physically remodel their microenvironment in 3D, even if they do not change cell morphology.[44] Hybrid LM/PEG hydrogels were designed with controlled degradability by using different VPM to PEG-AC ratios. VPM is a target sequence to several secreted proteases such as collagenase I. Therefore, hydrogel degradation will depend on the presence of cell-secreted MMPs. By varying the collagenase I concentration (10 and 30 U per ml), an enzyme that degrades LM and VPM, we observed that the degradation of 5% w/v LM521/PEG (AC:VPM, 2:1) depends on the collagenase concentration for the first 3 days. Then, data suggest that the hydrogels start to degrade also hydrolytically

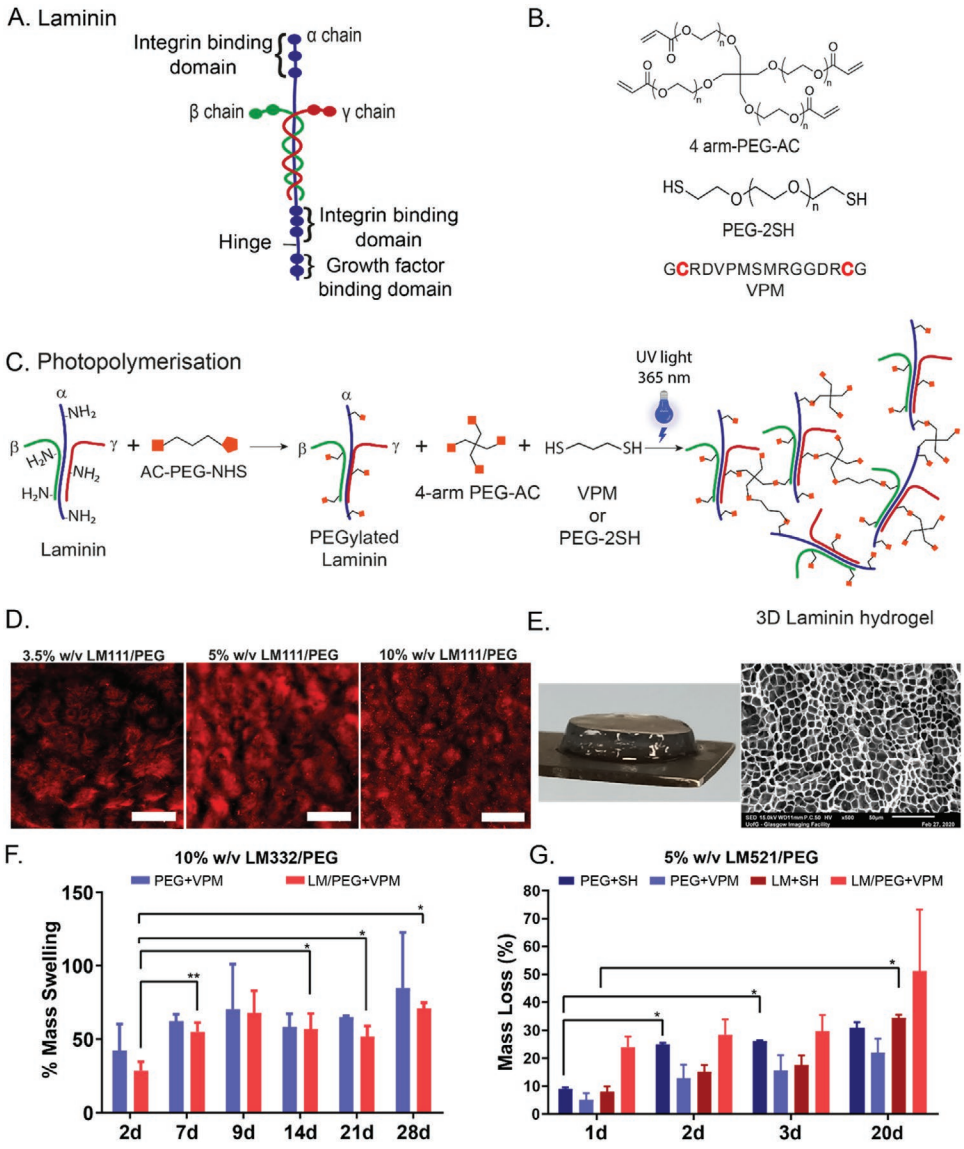

Figure 1. LM hydrogels chemistry and physical characterisation. A) LM structure with hypothesized GF binding sites. B) Gel components: 4-arm PEG AC macromer, PEG-2SH, and VPM, a target sequence to several secreted proteases. C) LM/PEG gel formulation schematic drawing, where the first step presented is PEGylation, the reaction used to functionalise LM molecules with ACs at different ratios, followed by photopolymerisation, reaction used to crosslink the LM-PEG gel. D) Immunofluorescence images of laminin distribution in 3.5, 5 and 10% w/v LM111/PEG gel cryosections (scale bar 50 µm). Laminin was stained with a Cy3 secondary antibody, shown in red in the images. E) Picture showing a flat LM/PEG hydrogel after polymerisation and SEM picture of the hydrogel network. F) Wet mass loss of 10% w/v LM332/PEG hydrogels incubated for 28 days in basal culture medium (mean ± standard deviation (SD), $n = 3$, a two-way ANOVA with Geissner–Greenhouse correction and Tukey post-hoc test was used to compare the PEG ± VPM and LM/PEG ± VPM data along the time series, with p values stated in the Supporting Information Table). Comparison between the samples within the same group are shown in Table S1G, Supporting Information. Degradation of LM521/PEG hydrogels with VPM (degradable gels) and SH (non-degradable gels) at AC:VPM or AC: SH ratio of 2:1 using 30 U per mL of collagenase type I (mean ± SD, $n = 3$, a two- way ANOVA test with a mixed-effects model to compensate for few missing values was performed between all the time points, followed by Tukey's post-hoc multiple comparisons test with p values stated in Table S1, Supporting Information). Comparison between the samples within the same group are shown in the Supporting Information Table.

after 20 days (Figure 1G; and Figure S4A, Supporting Information).

Next, to adjust the mechanical properties of the hydrogel for the different applications intended, LM/PEG hydrogels with different amounts of 4-arm PEG-acrylate (PEG-AC) at a final concentration of 3.5%, 5%, and 10% w/v were crosslinked with different ratios of PEG-AC to protease-degradable VPM, namely AC:VPM: 2:1,1:1, or 1:2. Degradability and mechanical properties of the system can be controlled independently by altering the ratio of the AC to VPM. By increasing the amount of PEG-AC, we obtained hybrid LM/PEG-gels with controllable stiffness of ≈2, 5, and 10 kPa, as measured by atomic force microscopy (AFM) and illustrated in Figure S3A, Supporting Information (left side). Since the amount of LM is tissue-dependent, we produced gels with different concentrations of LM while maintaining a constant stiffness (Figure S3A, right side, Supporting Information).[6] This

further corroborates the versatility of the system as stiffness can be controlled independently of the amount of LM or LM isoform.

To further expand the range of mechanical properties of the hydrogels, their composition was varied to achieve final concentrations of 12% and 15% w/v PEG (≈15kPa and 25kPa); and then crosslinking the network at 2:1 AC:VPM ratio. Mechanical properties of LM/PEG hydrogels were characterised by shear bulk rheology and nanoindentation (**Figure 2A**,C); these techniques allow investigation of distinct aspects of the mechanical properties of hydrogels, due to i) the length scale at which they are performed (bulk vs nanoscale), ii) the nature of the measurement (i.e., dynamic vs static), iii) the mode of deformation of the material (shear vs axial).[45]

Shear rheology measurements were performed to study the bulk viscoelastic (i.e., dynamic) properties of the gels which arise both from the intrinsic polymeric nature of the material as

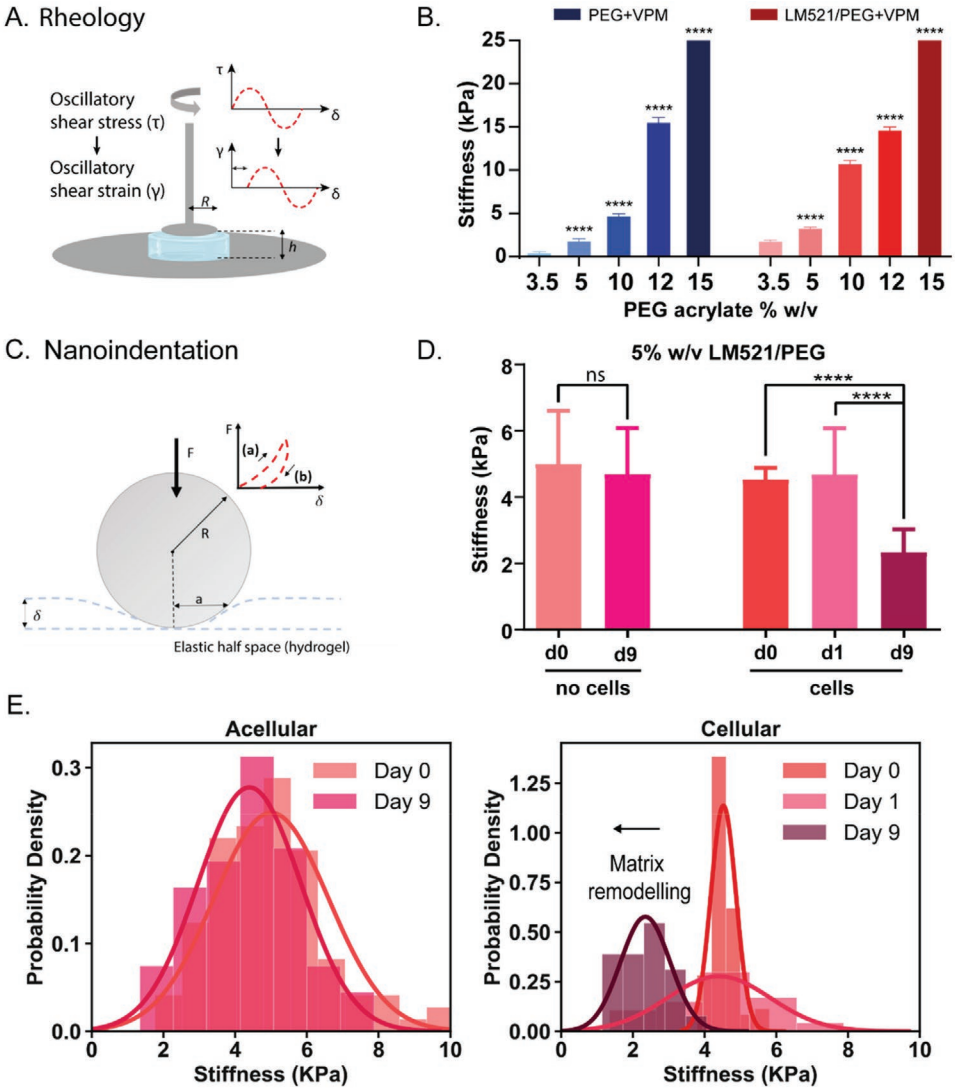

Figure 2. Mechanical Properties of LM/PEG hydrogels. A) Bulk rheology schematic (left side). The upper plate of radius *R* (7.5mm) oscillates at a constant frequency (10 rads^{-1}) and increasing shear stress, τ, resulting in an increasing oscillatory strain γ (0.01 to 1%). The phase lag, δ, between the applied stress and the resulting strain defines the viscoelastic behavior of the sample. B) Bulk rheology results. Each bar reports the mean of five consecutive data points of a strain sweep performed in the LVE region of the material at gap size corresponding to an applied force of 0.1N. Error bars report mean ± SD, $n = 1$ per gel. For each gel, five points ($n = 5$) were taken from a strain sweep to calculate *G'*. Significance calculated using one-way ANOVA with Tukey multiple comparison to compare different percentages of PEG with/without LM where ****$p < 0.0001$. Comparison between PEG gels with/without laminin with the same PEG percentage are shown in Table S1C, Supporting Information. Schematic of a nanoindentation experiment (left side). A spherical tip of radius *R* (8 µm) indents the hydrogel – modeled as an elastic half space – with force *F*, inducing a deformation field of characteristic size *a* and depth δ. By fitting the Hertz solution to the forward curve of the *F*–δ relationship (represented by (a) in inset schematic graph); (b) is the retract curve of the *F*–δ relationship), the Young's modulus is calculated (Equation (1) shown in Experimental Section). D) Nanoindentation results. In situ stiffness measurements of hydrogels loaded with hMSCs at 0, 1, and 9 days compared with an acellular sample measured after preparation at day 0 and 9 (mean ± SD, n > 22 curves, significance calculated using ANOVA with Tukey multiple comparison where ****$p < 0.0001$). E) Shows unimodal distribution of Young's Modulus (normalised histograms and probability function estimations of modulus distribution), in accordance with the literature,[46] as explained in the main text.

well as the high water content entrapped within the network.[46] Sufficiently robust bulk mechanical properties are essential to ensure material stability in vivo.[47] A frequency sweep was performed prior to all experiments to determine the regime where the shear storage modulus, *G'*, was independent of frequency, ω, so that the shear modulus G of the gels could be measured ($G = \lim_{\omega \to 0} G'(\omega)$).[48] Strain sweeps in the range of 0.01% to 1% at an angular frequency of 10 rad s^{-1}, within the linear viscoelastic (LVE) regime of the gels, were performed and the shear modulus determined at a gap size corresponding to a normal force of ≈0.1 N (see Experimental Section for more details). Rheology results are reported as stiffness (Young's modulus) throughout the manuscript to ease the comparison with nanoindentation (and AFM) results. The Young's modulus, E, was obtained from shear modulus, G, following $E = G(1+\upsilon)$, where, υ is the Poisson's ratio, assumed to be 0.5 (incompressible material) given the highly hydrated nature of the gels. Results are reported in Figure 2B for PEG + SH and LM521/PEG + VPM gels with the same ratio AC:VPM (2:1). Variation of PEG-AC content at final concentration of 3.5, 5, 10, 12, and 15% w/v allowed us to produce a wide range of stiffnesses, from very soft gels suitable for 3D culture of neural cells, for example, ≈2 kPa for 3.5% w/v LM521/PEG degradable;[33,34,36,49] to stiff gels suitable for osteogenic differentiation of stem cells, for example, ≈25 kPa (and up to ≈80 kPa; Figure S3B, Supporting Information) for 15% w/v LM521/PEG degradable.[45,50] The low frequency range and LVE regime of the measurements explain the increase in E with polymer concentration as a direct consequence of the increasing number of crosslinks in the network, following rubber elasticity theory,[48] and in accordance with PEG gels reported in literature.[51]

Establishing that the bulk mechanical properties of the hydrogels offer a wide range of physiologically relevant stiffnesses,[47] we moved on to investigate microscale properties of the gels which are important in the context of cell interactions with the material. Nanoindentation measurements allow investigation of the static properties (i.e., Young's modulus) of the gels at the microscale (see Figure 2C and Experimental Section for more details). However, the ECM is a dynamic environment involving active tissue mechanics driven by cells. Here, we investigated the mechanical properties of hydrogels loaded with human mesenchymal stem cells (hMSCs) using protease-degradable hydrogels (5% w/v LM521/PEG + AC:VPM (2:1) and demonstrate that a "biolabile" environment[47] permits cells to mechanically remodel their surroundings (Figure 2D). After 9 days in culture, the hydrogels' Young's modulus decreased by almost ≈50%. This suggests that hMSC-secreted MMPs cleave the degradable linker (VPM), thus leading to softening of the surrounding cellular microenvironment by a degradation-driven remodeling process. This is in accordance with recent literature,[44] where it was shown that sufficiently cross-linked hMSC-laden S-HA-PEGDA ("stiff" gels) exhibited a decrease in stiffness due to cell-driven matrix degradation; in contrast to weakly cross-linked gels ("soft" gels) where matrix deposition was dominant and led to an increase in hydrogel stiffness.

Our results are also in agreement with those of Ferreira et al.[44] in terms of Young's Modulus distribution. The Young's modulus is unimodally distributed when microenvironment remodeling is driven by degradation (as in this case, Figure 2E) whereas it takes on a bimodal profile when surrounding remodeling is driven by matrix deposition and therefore stiffening.[44] Matrix remodeling (i.e., both the deposition of a pericellular ECM and the degradation of the surrounding environment) is an important variable to consider in addition to initial mechanical properties of the biomaterial[44,52–54] as it has been shown that matrix deposition and degradation are a variable controlling hMSC phenotype.[44]

To assess the biocompatibility of LM/PEG hydrogels, hMSCs were encapsulated in 5% w/v LM 521/PEG hydrogels with an AC:VPM ratio of 2:1 and cultured for 1, 3, and 7 days, followed by live/dead mammalian cytotoxicity/viability assay. hMSCs cultured in 5% w/v LM521/PEG hydrogels showed viability values of approximately 75% after 7 days (**Figure 3A**; and Figure S5A, Supporting Information). Over the past few decades, cell morphology in 3D has been shown to be influenced by stiffness, degradability rate, and ECM-protein concentration in the material.[55,56] To evaluate whether the morphology of the cells is influenced by degradability rate, LM521/PEG gels at different ratios of AC:VPM (2;1,1;1,1:2) were loaded with hMSCs for 7 days. Figure 3B; and Figure S5B, Supporting Information, show that cell morphology is similar for all the different degradation ratios after 7 days, but cells are less rounded and display more protrusions per cells in the gel with higher degradability rate (e.g., 1:2 of AC:VPM ratio). The fact that the cell morphology did not change with increasing degradability after day 7 can be correlated to the hydrogel mesh size, as well as the chain growth polymerisation method used to prepare the hydrogel.[57]

These results agree with recent studies which showed that chain versus step-growth polymerizations impact cellular morphology and function.[58,59] The influence of the LM content on cell morphology was also studied. Gels with different concentrations of LM 521 (100 and 500 μg mL^{-1}) were prepared and compared with gels without LM521 after 7 days in culture. Our results indicate that LM521/PEG (2:1) hydrogels with different LM concentrations do not have an influence on hMSC morphology (Figure 3C; and Figure S5C, Supporting Information). This can be explained by the small mesh size of the hydrogels, which was calculated theoretically using hydrogels' stiffness shown in Figure S6, Supporting Information. That MSCs in 3D hydrogels do not change their morphology due to a small mesh size is in agreement with the work of Huebsch et al.[60]

2.2. 3D LM332/PEG Hydrogels Loaded with BMP-2 Underpin In Vitro Osteogenesis

Different LM isoforms have different affinities for various GFs[9] and the abundance of every LM isoform is tissue dependent,[24] suggesting that LM has tissue-specific roles.[61] In this work, our aim is to use lower concentrations of GFs in solid-phase presentation in 3D environments with controlled mechanics and degradability. Concentrations used in vitro are typically in the range of 50 to 100 ng mL^{-1} for 2D cultures [62,63] and up to 100 μg mL^{-1} in 3D cultures, specifically hydrogels.[64,65]

We first investigated whether BMP-2 loaded in LM332/PEG hydrogels is retained within the system as this LM isoform had shown a high affinity for BMP-2.[9] The GF-binding ability of

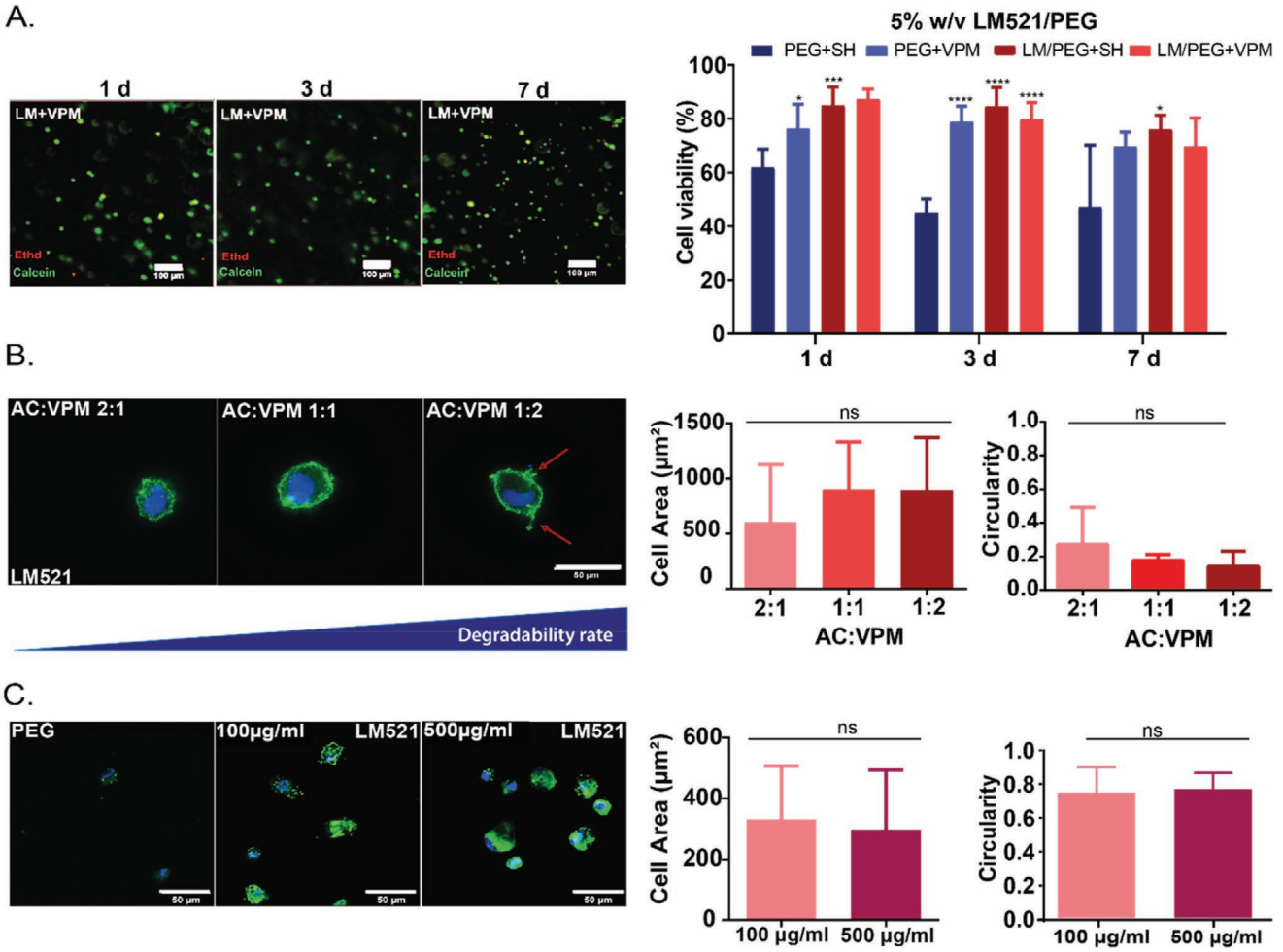

Figure 3. Cell viability and morphology of hMSCs in 3D LM/PEG hydrogels. A) Images of calcein (green) and ethidium (red) for hMSCs in 5% w/v LM521/PEG with 100µg mL^{-1} of LM521 at AC:VPM 2:1 and quantification of hMSCs viability in 5% w/v LM521/PEG hydrogels after 1, 3, and 7 days (scale bar 100 µm). The lowest viability values were found in the PEG+SH hydrogels, while in the LM/PEG gels, the viability values were higher than 75% in each tested condition (mean ± SD, $n = 3$, significance calculated using one-way ANOVA with Tukey multiple comparison for samples within the same group with $*p = 0.0219$, $***p = 0.0004$, $***p = 0.0001$). Comparison between samples within different groups are shown in Table S1B, Supporting Information. Immunofluorescence images of the actin cytoskeleton (green) and nuclei (blue) for hMSCs in 5% w/v LM521/PEG with 100 µg mL^{-1} of LM 521 at different ratios of AC:VPM (2:1, 1:1, 1:2) (scale bar 50 µm) with a display of protrusion in the images by using a red arrow and quantification of cell area and circularity for those images and C) 5% w/v LM521/PEG at 2:1 ratio with various LM concentration (100 to 500 µg mL^{-1}) compared with gels without LM after 7 days. Statistics are shown as mean ± SD, $n = 5$ images per condition from three different biological replicates (scale bar 50 µm). Data were analysed by an unpaired t-test, $\alpha = 0.05$ with no statistically significant difference found between the samples with $p > 0.05$.

the hybrid LM332/PEG hydrogels was investigated by loading hydrogels with 5 µg mL^{-1} BMP-2 labeled with AlexaFluor-488 dye. In **Figure 4A**, after 5 days, the release in 5% w/v LM332/PEG and PEG-only hydrogels shows that the former retained up to 85% of the initial amount of BMP-2, while the retention in PEG-only gels was lower, around 70%. In the 10% w/v LM332/PEG hydrogels, BMP-2 retention was similar to that seen at 5% w/v, whereas in 10% w/v PEG-only hydrogels, BMP-2 retention was slightly higher; 80% in the 10% w/v versus 70% in the 5% w/v hydrogels. We hypothesise that the higher retention of BMP-2 in LM/PEG hydrogels is due to BMP-2 being bound to LM which recapitulates binding of GFs to the ECM and should result in stronger biological effects.[66] The observed retention of BMP-2 in PEG-only gels is likely due to the mesh size of the system, which leads to lower swelling of the hydrogel and less diffusion of BMP-2 over 5 days. We hypothesise that even if BMP-2 is sterically retained within the hydrogel, this is in "soluble presentation", that is, not bound to the ECM and so with lower biological activity.

Our release results are in accordance with the literature, where fibrin gels functionalized with heparin, which is known to bind GFs, were loaded with BMP-2 and retained 85% of the initial GF amount.[67] BMP-2-loaded collagen gels, that are currently the gold standard in vivo,[68] released 90% of their initial payload after 5 days. Overall, data suggests that BMP-2 binds to the full-length LM molecule crosslinked to the 3D PEG hydrogels, which can be produced with controllable stiffness and degradation rate. Moreover, LM ability to bind BMP-2 in a dose-dependent manner was demonstrated by studying the release of BMP-2 at different concentrations (0.1, 1, and 5 µg mL^{-1})

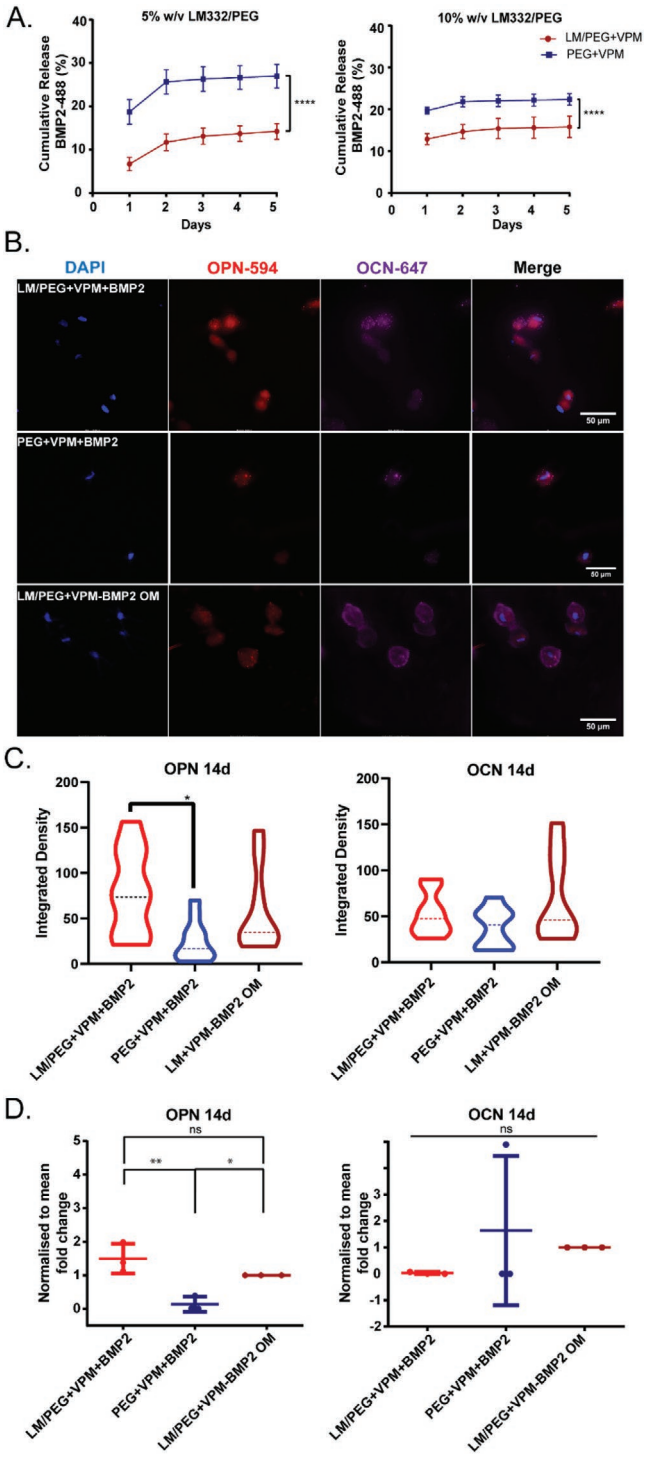

Figure 4. LM/PEG promotes hMSCs osteogenesis in 3D A) Cumulative release of fluorescently labeled BMP-2 with Alexa 488 (BMP-2-488), from 5 and 10% w/v PEG and LM332/PEG hydrogels, loaded with 5 µg mL^{-1} BMP-2-488 over 5days (mean ± SD, $n = 3$, ****$p < 0.0001$, Kruskal–Wallis and Dunn's post hoc test). B) Immunofluorescence images of hMSCs cultured for 14 days in 10% w/v LM332/PEG in culture medium, under basal and differentiation conditions (osteogenic media-OM). Images show nuclei (blue), osteopontin (red), osteocalcin (magenta) (scale bar 50 µm). C) 3D immunofluorescence quantification of osteopontin and osteocalcin from z-stack images (mean ± SD, $n = 3$,5 stacks per replicate) using Imaris. We have represented in the graph the Integrated density (total raw intensity per image normalised by cell area), rendered in 3D Imaris for each imaged volume. Significance calculated using one-way ANOVA with Tukey multiple comparison, where *$p = 0.0116$. D) Real-time qPCR analysis for markers of osteogenesis (OPN and OCN) after 14 days. Each condition was normalised to the osteogenic media (OM) (mean ± SD, $n = 3$, one-way ANOVA with Tukey multiple comparison, where **$p = 0.0027$, *$p = 0.0236$).

from 10% w/v LM332/PEG over 5 days (see figure S7, Supporting Information).

We next investigated the ability of hybrid LM332/PEG hydrogels to promote osteogenic differentiation of hMSCs. To test this hypothesis, hMSCs were embedded in 3D LM/PEG hydrogels loaded with 5 µg mL^{-1} BMP-2 and cultured for 14 and 21 days to assess their phenotype, in both basal and osteogenic media (OM). At initial loading, the amount of BMP-2 in a typical gel was 0.25 µg, after 5 days it was 0.22 µg. The molecular weight of LM332 is 619 kDa and is 26 kDa for the BMP-2 dimer. Thus, the stoichiometric ratio of BMP-2 to LM332 is initially ≈2 and ≈1.7 after 5 days of release; the amount of BMP-2 loaded in the hydrogels used is enough to bind all the LM molecules in the system.

Figure 4B shows immunofluorescence images of hMSCs cultured for 14 days under basal and osteogenic conditions to evaluate the expression of the late osteogenic expression markers osteopontin (OPN, in red) and osteocalcin (OCN, in magenta). Detailed immunofluorescence images displayed in Figure 4B were added to Figure S8A, Supporting Information, for better visualisation. To quantify the total surface volume and intensity of OPN and OCN expression for cells cultured for 14 days, 3D surface rendering of z-stacks with Imaris software was employed (see Experimental Section). It was observed that the presence of BMP-2 in LM332/PEG increased OPN expression to levels comparable to gels cultured in osteogenic media (Figure 4C), without any effect on OCN expression after 14 days (Figure 4C). On the other hand, PEG-only gels loaded with BMP-2 showed lower expression of OPN and OCN compared to gels loaded with BMP-2 and cultured in osteogenic media. These data demonstrate that the amount of soluble BMP-2 that remains trapped in the PEG network (PEG+VPM+BMP2) is not enough to promote osteogenic differentiation whereas the same amount of BMP-2 bound to LM is.

To confirm this, gene expression of osteogenic markers was also assessed by qRT-PCR. Results showed upregulated osteopontin expression when compared to the gels cultured in osteogenic media at 14 days (Figure 4D), as previously observed.[69] OPN and OCN expression were further evaluated after 21 days, indicating that OCN expression level did not show any statistically significant difference between the two tested conditions (Figure S8B, Supporting Information). The lack of statistical significance in the mRNA expression values of OPN and OCN at 21 days might be due to the temporal expression profile of both genes,[69] where OPN reaches a maximum around 14 days and then the expression is attenuated, whereas OCN shows a monotonic increase in its expression values, reaching a maximum after 21 days. Even if the amount of BMP-2 retained in the gel after 5 days is similar (220 and 200 ng corresponding to LM/PEG and PEG), the biological effects of the BMP-2 bound to LM332 on the

hMSC differentiation are significantly different. We hypothesize that this effect is due to the synergistic effect between LM and BMP-2, as a result of a solid-phase presentation of BMP-2 bound to LM, compared to the effects of BMP-2 in "soluble" presentation. This results in hMSC phenotypic changes as demonstrated by immunofluorescence and qPCR (Figure 4B,C,D).

2.3. LM411/PEG Hydrogels Loaded with β-NGF Promote 3D Neurite Outgrowth

We investigated the capacity of LM411-based hydrogels to bind and present β-NGF to explanted dorsal root ganglion (DRG) cell cultures in a 3D environment. DRG cells are a cluster of neurons located in the dorsal root of the spinal nerve. Being afferent cells that carry sensory messages to the CNS, they are associated with neuropathic pain.[70] In particular, this neuron cluster is in charge of regulating important processes associated with nocioception and temperature sensing, inflammarion, and somatic pain as well as neuropathic pain (NP). These neurons are inherently involved in peripheral nerve injury repair and neurodegenerative disorder management as they bridge communication between the PNS and CNS. Thus, it is important to restore nerve function and communication of the two systems in the case of traumatic injury or disease.

For this work, we explored the behaviour of explanted DRG cells from P1 rat pups (**Figure 5A**) when introduced to 3.5% w/v PEG+VPM, LM411/PEG+VPM and FN/PEG+VPM soft hydrogels, as they are better suited for neural regeneration applications,[34,49] with or without added GFs. The same concentration of LM and FN was incorporated in the PEG hydrogels (i.e., 0.3 mg mL^{-1}) in order to obtain an accurate comparison of their biological activity.

For stimulating neurite growth in DRG cultures, the LM411 isoform was used as it is one of the two LMs (LM211 and LM411) expressed in peripheral nerves, and its growth-promoting qualities for ganglion neurons after injury have previously been reported.[71] In the work of Plantman et al., neurite growth on LM411 was said to be β-NGF dependent.[71] This is reasonable, considering that this β-NGF is heavily secreted by the peripheral nerve niche when injury occurs to promote local neuronal survival and axonal regrowth.[72] To asses the role of LM411 hydrogels in driving neurite outgrowth, hydrogels prepared with another key ECM protein, FN, were also employed. In the past, FN has been used to promote Schwann cell response,[73] and these cells have known roles in providing axons of injured nerves with metabolic and trophic support.[74] The role of FN in promoting neurite extension in vitro in hydrogel substrates has long been established as this ECM protein is intrinsically linked with the adhesion of the cell to the surface. In the past, FN has shown to aid nerve fiber extension and regeneration in 2-hydroxymethylacrylate hydrogels (HEMA),[75] silk fibroin hydrogels,[76] and FN-patterned comb polymers, for example.[77]

To gain insights on whether our system could drive neurite growth by efficiently presenting β-NGF via ECM proteins, the GF was introduced into the experimental system in two ways: within the hydrogel precursosrs before polymerisation (at a concentration of 1 μg mL^{-1}) or dissolved in the media (at a concentration of 0.5 μg mL^{-1}, media was changed every 2 days). Explanted DRGs were cultured and fixed for immunostaining at 7 days (Figure 5B); neurite extension was subsequently assessed by the maximum number of neurites per sample (Nmax)[78] obtained with Neurite-J, an ImageJ plug-in (Figure 5C; and Figure S9, Supporting Information).

It was clearly observable that DRGs cultured in LM411/PEG+VPM hydrogels with 1 μg mL^{-1} of β-NGF inside the gel (before polymerisation) showed the most neurite outgrowth. When compared to PEG+VPM hydrogels with β-NGF loaded inside the gel, LM411/PEG+VPM with β-NGF loaded inside the gel showed significant neurite outgrowth (Figure 5B); the same was seen with FN/PEG+VPM hydrogels with β-NGF inside the gel. Neurite outgrowth was also significantly greater when β-NGF was introduced inside the gel before polymerisation, compared to conditions with β-NGF added into the media; this is especially true of the LM411/PEG + VPM condition ($p = 0.0002$). This result suggests a role for LM in presenting β-NGF efficiently to the cell, driving greater growth by binding and releasing β-NGF in a time-efficient manner, which propells greater neurite growth than when β-NGF is added to the media. Additionally, when contrasting the two ECM proteins, LM411/PEG+VPM hydrogels showed an increased Nmax when compared to FN/PEG+VPM ($p = 0.1527$). Although not statistically significant ($0.1527 > 0.05$); these results still suggest a stronger role for LM411 in aiding neurite outgrowth than FN; this corroborates previous literature that highlights the role of this ECM protein in driving greater neuron sprouting than FN.[79–81]

2.4. Outlook

We have developed a platform of engineered hydrogels that incorporate full-length LM within a synthetic polymer network with controlled physico-chemical properties. Cells reside within the ECM, a collection of proteins, such as FN and LM, which plays an important role in guiding cell fate and providing mechanical support for cells. Critically, these proteins hold great potential in tissue engineering due to their ability not only to support cell adhesion but for their ability to bind a large range of GFs;[9,31] many hydrogels fail to recapitulate this key niche facet. These properties highlight the importance of incorporating full-length proteins in biomaterials aimed at tissue regeneration and repair applications.

In contrast to FN, that has only two isoforms, alternative mRNA splicing of LM can produce up to 16 isoforms whose abundance is tissue-dependent and in turn have the ability to bind different GFs, making them a more versatile candidate than FN. LMs influence cell differentiation, migration, and phenotype stability and inhibit apoptosis by signalling via cell membrane receptors such as integrins and dystroglycans.[6] Due to their involvement in the development of various tissues as a component of the BM, LMs were reported to promote the regeneration of muscle, skin, liver and nerves both in vitro and in vivo.[14,82–84]

To capitalise on these advantages and to form a tuneable system, we combine LM with PEG, a synthetic polymer whose structure allows to produce hydrogels with defined stiffness, as shown in Figure 2B,D,E. Furthermore, we note that tissue development requires matrix remodeling by cells, that is conducted

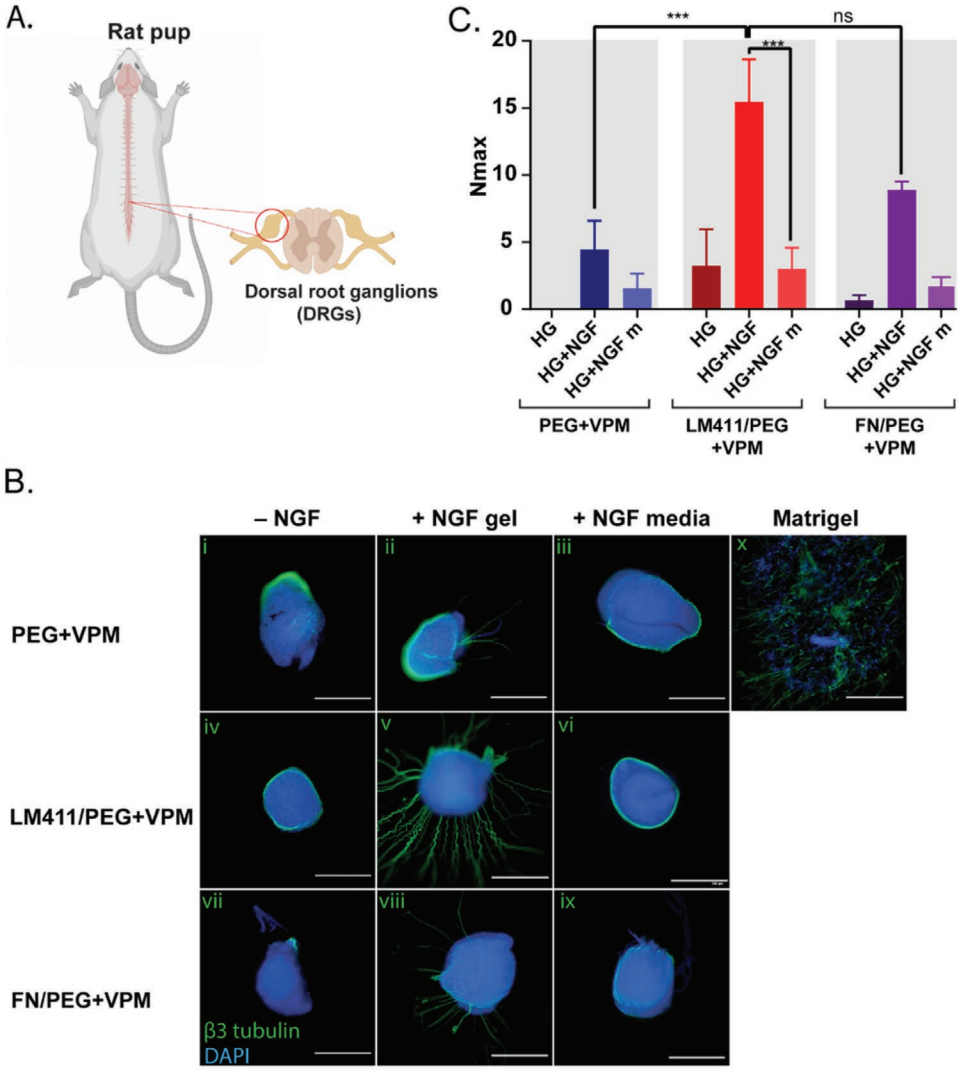

Figure 5. LM/PEG enhances neurite growth in 3D. A) Schematic drawing of DRGs positioned in the spinal cord of a rat pup. B) Representative images of DRG cells in diverse culture conditions i–x): i) PEG+VPM hydrogel (HG) with no β-NGF added, ii) PEG+VPM hydrogel with 1 µg mL^{-1} β-NGF added in the gel (HG+NGF), iii) PEG+VPM hydrogel with 0.5 µg mL^{-1} β-NGF supplemented media (HG+NGF m), iv) LM411/PEG+VPM hydrogel with no β-NGF added (HG), v) LM411/PEG+VPM hydrogel with 1 µg mL^{-1} β-NGF added in the gel (HG+NGF), vi) LM411/PEG+VPM hydrogel with 0.5 µg mL^{-1} β-NGF supplemented media (HG+NGF m), vii) FN/PEG+VPM hydrogel with no β-NGF added (HG), viii) FN/PEG+VPM hydrogel with 1 µg mL^{-1} β-NGF added in the gel (HG+NGF), ix) FN/PEG+VPM hydrogel with 0.5 µg mL^{-1} β-NGF supplemented media (HG+NGF m), x) Matrigel positive control. C) Neurite growth analysed by Neurite-J in three independent experiments ($n = 3$). Nmax represents the maximum number of neurites found in each sample. Each condition is represented by three replicates (mean ± SD, n = 3-individual experiments; ***$p = 0.007$ (PEG+VPM+NGF inside versus LM411/PEG+VPM+ NGF inside), *** $p = 0.002$ (LM411/PEG+VPM+NGF inside vs LM411/PEG + VPM+NGF media), *$p = 0.1527$ (LM411/PEG+VPM+NGF inside vs FN/PEG+VPM+NGF). Scale bar = 500 µm.

by matrix-degrading enzymes like collagenase, trypsin, and other MMPs. Since PEG can only be degraded hydrolytically and not enzymatically, we show that the addition of protease-degradable peptides can modulate the enzymatic degradability of the hydrogel (see Figure 1G). While developing hydrogels, we considered other parameters affecting degradation rate such as the mesh size and swelling properties of the hydrogel as shown in Figure 1F; and Figure S5, Supporting Information.[57]

Recent studies have used LM111 combined with PEG in a 3D hydrogel. For example, Francisco et al. explored how soft, 3D LM111-functionalized hydrogels can promote the regeneration of the nucleus pulposus region of the intervertebral disc.[25,28] However, the authors did not take advantages of the versatility of LM isoforms, being able to bind different GFs in a tissue-dependent manner.

Ishihara et al. showed that the covalent incorporation of an engineered GF-binding domain derived from LM, α2PI1–8-LAMA33043–3067, in a 3D fibrin matrix, significantly enhanced the effect of VEGF-A165 and PDGF-BB on skin wound healing, by increasing GF retention into fibrin both in vitro and in vivo.[9] While this work set the concept of GF binding to LM at low doses, their approach included the use of a short fragment of LM's alpha chain, without taking advantage of the full biological functions of the whole LM molecule.

A more recent study[33] demonstrated the potential of a 4-arm-PEG-Maleimide (PEGMAL) hydrogel modified with affinity-bound LM as a dynamic 3D platform enabling NSCs proliferation, neuronal differentiation, and neurite extension. The authors present a strategy to bind LM to a PEG backbone using agrin, a large proteoglycan that binds to LM through its N-terminal domain. Our approach, in turn, provides a robust and reliable system by covalently binding LM to the PEG network and incorporating GFs that enhance cell growth and differentiation.

Here, we present a novel approach combining the different strategies discussed above to incorporate several LM isoforms (521, 332, and 411) as native, full-length proteins. PEGylated LM molecules are then covalently crosslinked to 3D PEG backbone for an efficient and long-term display and delivery of GFs to the resident cell population (BMP-2 and β-NGF) (Figure 4A).

Overall, the BMP-2 and β-NGF-sequestering systems developed in this study improve the activity and efficiency of GF delivery in reduced doses and prevent the need for their exogenous administration to guide stem cell fate and neurite outgrowth, as shown in Figures 4 and 5.

3. Conclusion

Here, we report the development and characterization of a platform based on hybrid 3D LM-PEG hydrogels with tuneable mechanical properties and degradability, as well as highly efficient GF presentation for tissue regeneration of bone and nerve tissue. The LM/PEG hydrogels with GFs presented in this work introduce a flexible platform to engineer biomimetic microenvironments with tissue-specific biological and mechanical properties, with the potential to support the rational design of next generation in vitro tissue models.

4. Experimental Section

LM PEGylation: LMs (Biolamina AB), 100 µg mL^{-1}) were PEGylated using PEG-AC-SCM (5 kDa, Laysan Bio, Inc). LM PEGylation was carried out to introduce functional AC groups to the protein. LM 411 (579 kDa, Biolamina AB), LM 521 (762 kDa, Biolamina AB), LM 332 (619kDa, Biolamina AB), and LM 111 (810 kDa, Trevigen Inc.) were PEGylated according to their respective molecular weights. The PEGylation (Figure 1C top) was done at a 1:25 molar ratio of LM to PEG-AC-SCM. The LMs came in a phosphate-buffered saline (PBS) solution at 100 µg mL^{-1}. Thus, 500 µl of the proteins were dialysed to change the buffer to sodium bicarbonate (NaHCO3; pH 8.5 as PEGylation takes place at this pH). To obtain the desired 1:25 molar ratio of AC to LM, calculated volumes of the Ac-PEG-NHS (1 mg mL^{-1} in PBS) were added to the respective LM solution and left to mix for 2 h at RT. Then, the solution was dialysed to remove all the unreacted acrylates and change the buffer to PBS for 1h at 4 °C. The LM PEGylated was stored at -20 °C for future use.

FN PEGylation: FN (YOProteins, 3 mg mL^{-1}) was PEGylated as described by ref. [41]. FN was denatured in denaturing buffer (5 mM Tris[2-carboxyethyl]phosphine hydrochloride [TCEP], pH 7, Sigma) and 8 M urea (Acros Organics, 99.5%) in phosphate buffer saline (PBS, Gibco, pH 7.4) for 15 min at RT. After that, (PEGMAL; 20 KDa, LaysanBio) was incubated for 30 min at room temperature at a molar ratio of 1:4 FN to PEGMAL. After obtaining PEGylated protein, non-reacted cysteine residues were blocked by alkylation using 14 mM iodoacetamide (Sigma) in PBS at pH = 8. Then, the product of the blocking reaction was dialysed in PBS for 1 h at RT. The dialysed protein solution was precipitated by adding 9 volumes of cold absolute ethanol to the protein solution. This was then mixed and incubated overnight at –20 °C. The next day, the protein solution was centrifuged at 15 000 g and 4 °C for 15 min. The supernatant was discarded and the pellet was washed once more in cold ethanol (90%) and centrifuged at 15 000 g and 4 °C for 5 min. Pellets were then dried and dissolved using 8 M urea to achieve a final protein concentration of 2.5 mg mL^{-1}. Once the protein was dissolved, the solution was dialysed in PBS one last time and stored at -20 °C for future use.

3D LM/PEG Preparation: Different LM PEGylated isoforms were mixed with various amounts of 4-arm PEG-acrylate (PEG-AC,10 kDa, Laysan Bio, Inc.), a protease degradable peptide cross-linker GCRDVPMSMRGGDRCG (VPM, 1.7 kDa, GenScript), and a photoinitiator (0.1% w/v Irgacure 2959, Sigma–Aldrich) to obtain degradable hydrogels with different stiffness. To from non-degradable hydrogel, VPM volumes required were substituted with PEG dithiol (SH-PEG-SH, 2 kDa, Creative PEGWorks) as they have the similar molecular weight. The thiolated crosslinker was added at different molar ratio of acrylate:thiol (AC:VPM) such as 2:1, 1:1, and 1:2 to obtain hydrogels with various degradability. Subsequently, the hydrogel mixture was immediately pipetted into custom sterile polydimethylsiloxane (PDMS) molds (holes with 6 mm diameter and 3 mm thickness) and polymerised upon exposure to UV light (365 nm, Omnicure S1500, Excelitas Technologies, US) of power ≈5 mW cm^{-2} for 6 min (Figure 1C bottom). Synthesised hydrogels were then transferred to sterile non-tissue culture treated plate wells. The nomenclature used in this paper is x % w/v LM (γ)/PEG, *x* being the percentage of PEG used and γ is the LM isoform incorporated inside of the hydrogel.

Rheology Measurements: A stress-controlled rheometer (MCR302, Anton Paar) equipped with a parallel plate geometry (upper plate diameter 15 mm; gel diameter 17.2 mm) at a temperature of 23 °C was used. Sample hydration was maintained during measurements by addition of PBS at the exposed sides of the specimens. A frequency sweep was performed prior to all experiments to determine the regime where the shear storage modulus, G', was independent of frequency, ω, so that the shear modulus G of the gels could be measured ($G = \lim_{\omega \to 0} G'(\omega)$).[47] Strain sweeps in the range of 0.01% to 1% at an angular frequency of 10 rads-1, within the LVE regime of the gels, were performed and the shear modulus determined at a gap size corresponding to a normal force of ≈0.1 N for all gels reported in Figure 2. Additionally, a series of strain sweep tests were performed at different levels of compression: tests were performed by gradually varying the normal force applied to the unconfined samples (one strain sweep per level of compression), starting from a minimum force value of ≈0.1 N and with a minimal delay (i.e., of the order of a few seconds) between sequential compressions (Figure S3B, Supporting Information). In all tests, samples' hydration was maintained by addition of PBS at the exposed sides of the specimens.

Nanoindentation Measurements: Nanoindentation measurements were performed using a nanoindentation device (Chiaro, Optics11) mounted on top of an inverted phase contrast microscope (Evos XL Core, Thermofisher) following a previously described approach.[85] Measurements were performed at RT in culture media. For each sample, single indentation curves ($n > 22$) were acquired at a speed of 2 µm s^{-1} over a vertical range of 10 µm, changing the *(x, y)* point at every indentation. The selected cantilever had a stiffness of 0.032 Nm^{-1} and held a spherical tip of 8.0 µm radius. The collected curves were analysed using a custom Python code.[86] Curves were first aligned using a baseline detection method based on the histogram of the force signal[87] and the corresponding indentation was calculated for each curve. The Hertz model (Equation (1) and Figure 2C) was fitted to the forward curve of the force (F)-indentation (δ) curve up to an indentation of about 10% of the tip radius (R), and the Young's modulus (E) therefore extracted. The Poisson's ratio (υ) was assumed to be 0.5 as previously described.

$$F = \frac{4\,E\,\delta^{\frac{3}{2}}R^{\frac{1}{2}}}{3(1-\upsilon^2)} \quad (1)$$

Release of GFs: To determine the mass percentage release of BMP-2 (26 kDa, recombinant human bone morphogenetic growth factor, R&D Systems, Bio-Techne) from LM332/PEG hydrogels, BMP-2 was conjugated to with NHS-AlexaFluor-488 dye (10 µg mL^{-1}, Gibco-Life Technologies) to allow its detection using a fluorescence plate reader. Synthesised hydrogels were transferred to individual centrifuge tube filters (Eppendorfs with filter units, Corning Costar spin-X) loaded with PBS as a releasing buffer. Over 5 days, the tubes containing the hydrogels loaded with BMP-2 were centrifuged at a rate of 8000 rpm for 10 min once per day. The supernatant was collected and stored at –20 °C and the filter units were reloaded with 400 µL of PBS. Ultimately the supernatant aliquots were pipetted into a black non-tissue culture treated plate and the fluorescence intensity of the GF released from the hydrogels was measured at 490 nm excitation and 510–570 nm emission wavelength using a microplate reader (Modulus II Microplate Multimode Reader, Turner BioSystems). The concentration of BMP-2 in the samples was quantified using a standard curve, which relates fluorescence intensity to BMP-2 concentration, obtained from serial dilution of BMP-2 solutions.

MSCs Culture: Human bone marrow mesenchymal stem cells (hMSCs) (PromoCell GmbH, Germany) were expanded and maintained (Dulbecco's modified Eagle medium (DMEM) (Sigma–Aldrich), 10% FBS (Sigma), 1% Sodium Pyruvate (11 mg mL^{-1}, Sigma), 1% Gibco MEM NEAA (non-essential amino acids, Thermo Fisher Scientific), 2% antibiotic (6.74 U mL^{-1} penicillin–streptomycin (Sigma), and 0.2 µg mL^{-1} fungizone) (Sigma). Media was changed every 3 days. When 80% cells were confluent, they were detached from the culture flask using Trypsin-EDTA and spun down at 1400 rpm for 5 min. Cells were resuspended in PBS prior their encapsulation into the 3D hydrogels.

LIVE/DEAD Viability Assay: The viability of cells incorporated in LM/PEG hydrogels was assessed with the LIVE/DEAD Viability/Cytotoxicity Assay Kit (Thermo Fisher Scientific, UK) using calcein and ethidium homodimer (EthD1). Calcein labeled live cells with green fluorescence, whereas EthD labelled dead cells with red fluorescence. LM/PEG hydrogels were synthesised as described earlier (with the concentration of hMSCs encapsulated being equivalent to 1×10^6 cells per mL). At each time point, gels were washed with PBS twice, and appropriate volumes of calcein (4 mM) and EthD (2 mM) were added. After staining, gels were left to incubate for 30 min at 37 °C. To determine the percentage of cells viable in the culture, gels were consequently imaged using a fluorescent microscope (Zeiss Axio Observer.Z1-Inverted Microscope, US) on days 1, 3, and 7. Images acquired were processed using Fiji software, to calculate the number of viable cells in relation to the total number of cells (%).

Cell Morphology: Cells were fixed with 4% paraformaldehyde (PFA) for 15 min at RT and then permeabilized with 0.1% Triton X-100 for 10 min, before washing with PBS twice. After that, 1% bovine serum albumin (BSA, Sigma–Aldrich) in PBS was added to block non-specific antibody binding. Cell F-actin was labelled for 1 h incubation at RT with Alexa Fluor 488 Phalloidin (1:100, ThermoFisher) in blocking buffer. Nuclei were stained using Vectashield mounting medium with DAPI nuclear stain (Vector Laboratories). Samples were then washed in PBS three times. Z-stack imaging was performed using a Widefield microscope (Leica DMi8 Inverted Microscope) with a 40X/1.4 numerical aperture oil objective, and more than five images per condition of the three independent experiments were assessed using Fiji software to measure the cell morphology.

hMSCs Differentiation in 3D LM/PEG: Cell were encapsulated in LM/PEG hydrogels (1×10^6 cells per mL, $n = 3$) were incubated for 14 and 21 days in OM at a ratio of AC: VPM of 1:2, that was exchanged every 3–4 days. OM was prepared by mixing DMEM expansion media, supplemented with 100 µmol ascorbic acid (Sigma), 100 nmol dexamethasone (Sigma), and 3mM sodium phosphate (Sigma). After culture, hydrogels were fixed in 4% (v/v) PFA in PBS for 20 min and washed in PBS there times. Then, samples were treated with 0.1% (v/v) Triton-X-100 and 0.1% (v/v) Tween-20 for 15 min at RT. Cells were incubated for 1h with the following antibodies: OPN (1:400, ab8448, Abcam) and OCN (1:50, sc-390877, Santa Cruz Biotechnology). Detection was performed using the following secondary antibodies: Cy3 goat anti-rabbit (1:100, 16870-AAT, Jackson ImmunoResearch – Stratech), Alexa Fluor 647 donkey anti-mouse (1:200, Invitrogen).Nuclei were visualized with DAPI (0.5 µg mL^{-1}; D1306, Invitrogen) and F-actin with Alexa Fluor488 phalloidin (1:100 dilution, Invitrogen) incubated for 1h at RT. Z-stack imaging was performed using a Widefield microscope (Leica DMi8 Inverted Microscope) with a 63X/1.4 numerical aperture oil objective, and more than 30 cells from three independent experiments were assessed using Imaris software to quantify the mean intensity of the OPN and OCN.

Protein (OPN and OCN) Expression Quantification using Imaris: The Z-sections of the deconvolved images (20 slices) acquired from the widefield microscope were imported into Imaris 9.1.2 software (Bitplane AG, Zurich, Switzerland) and each part of the cell stained were quantified by 3D surface rendering. Briefly, the image display was adjusted for all of four channels (dapi, blue; phalloidin, green; OPN, red; OCN, magenta), and the rendering quality was set to 100%. Surfaces were created by selecting source channel and smooth surface detail set at 0.198 µm. Background subtraction was set to 0.743 µm, and the threshold was reduced for surfaces to fully cover all voxels. The surface area, volume of the surfaces, and mean intensity generated were quantified by Imaris for all the channels, and the values were exported into Excel for graphical and statistical analysis using GraphPad Prism. In certain cases, in the phalloidin channel, cells were in contact with each other, preventing an accurate rendering of individual cells and the quantification of their morphological parameters.

Quantitative Polymerase Chain Reaction with Reverse Transcription (qRT-PCR): Total RNA was extracted from MSCs cultured for 14 or 21 days under different experimental conditions using FastPrep Lysing Matrix D kit (MP biomedicals). Hydrogels were transferred into Lysing Matrix H tubes and 500 µl of trizol reagent (Invitrogen were added) on top of them. Then, the samples were homogenized in Lysing Matrix H tubes (MP Biomedicals, USA) on a FastPrep–24 (MP Biomedicals, 4.5 m s^{-1} for 2 cycles of 20 s). 0.1 mL of chloroform was added to each tube, shaken vigorously, and incubated RT for 2 min. Samples were then centrifuged at 12 000 g for 5 min at 4 °C to separate each sample mixture into a lower phenol–chloroform and an upper aqueous phase. The aqueous phase was carefully aspirated from each sample and placed into a clean eppendorf tube to carry out RNA isolation. In the aqueous phase 5 µl of a 3 mg mL^{-1} of solution GlycoBlue (Thermo Fisher Scientific) solution was added to each sample followed by 250 µl of isopropanol. Glycoblue is a blue dye conjugated to glycogen. Glycogen is precipitated with RNA in alcohol and its addition serves as a means of visualising RNA by way of producing a blue pellet during the extraction procedure. Samples were mixed by inverting each tube lightly and then incubated RT for approximately 10 min. After incubation, samples were centrifuged at 12 000 g for 10 min at 4 °C. The supernatant was aspirated to waste and the pellet washed in 500 µl of 75% ethanol solution. Samples were then centrifuged at 7500 g for 5 min at 4 °C to draw down the pellet. The supernatant was aspirated to waste and the pellet allowed to air dry. The pellet was then resuspended in 15 µl of RNase free water and incubated for 10 min on a heat block set to 55 °C to dissolve the RNA. Samples were stored at –80 °C until ready for use. RNA quantity and integrity were measured with a NanoDrop 1000 (ThermoScientific). Then 100 ng of RNA were reverse transcribed using the Superscript III reverse transcriptase (Invitrogen) and oligo dT primer (Invitrogen). Real-time qPCR was performed using Sybr select master mix and 7500 Real Time PCR system from Applied Biosystems. The reactions were run at least in triplicate for both technical and biological replicas. The primers used for amplification were designed from sequences found in the GenBank database and included: Runx2 (Forward: 5′-TGA GAG TAG GTG TCC CGC CT-3′, Reverse: 5′-TGT GGA TTA AAA GGA CTT GGT GC-3′) and OPN (Forward: 5′-TTT GCC TGT TTG GCA TTG C-3′, Reverse: 5′-TGG GTG CAG GCT GTA AAG CT3′) for osteogenic differentiation. GAPDH (Forward: 5′-GTG TGA

ACG GAT TTG GCC GT-3′, Reverse: 5′-TTG ATG TTA GTG GGG TCT CG-3′) was used as a housekeeping gene. The fractional cycle number at which fluorescence passed the threshold (Ct values) was used for quantification by the comparative Ct method. Sample values were normalized to the threshold value of housekeeping gene GAPDH: $\Delta C_T = (experiments) - C_T(\text{GAPDH})$. The Ct value of the control was used as a reference. $\Delta\Delta C_T = \Delta C_T(experiment) - \Delta C_T(control)$. mRNA expression was calculated by the following: $fold\,change = 2^{-\Delta\Delta C_T}$

Dorsal Root Ganglia: DRG cells were extracted from the isolated spine of P1 old rat pups. DRG cells were extracted from P1 rat pups as described by ref. [80]. P1 rat pups were donated from the Glial Cell Biology Group within the Institute of Infection and Immunity and Inflammation of the University of Glasgow. The provided tissue came from animal experiments carried out at the University of Glasgow, under projects approved by the Home Office in the UK. The spinal cord of each rat pup was isolated, and the adjacent tissues were removed. The spinal cord was cut in half in order to remove the cerebrospinal fluid. Each DRG was removed with sharp edged thumb forceps under a dissection microscope and collected in culture dishes. Dissected DRGs were placed in fresh Hank's balanced salt solution (Sigma). The excess meninges and tissue debris were removed with tweezers and surgical scissors under a dissecting microscope. DRGs were collected in petri dishes and introduced to 3.5% w/v PEG+VPM, LM411/PEG+VPM and FN/PEG+VPM hydrogels at one DRG per gel on the same day before polymerisation with a 0.5 mm gauge needle. For DRG in 3D culture, media was changed every 3 days.

Immunofluorescence, Image Acquisition, and Analysis for DRGs: DRG hydrogels were fixed with 4% PFA at RT for 20 min and stained with anti-β3-tubulin (ab78078). 2D Images for analysis were taken at 5X for DRGs using brightfield and fluorescent microscopy (ZEISS Axio Observer.Z1). Images were analysed with Neurite-J plug-in for ImageJ software. Graphs and subsequent statistical analysis were performed using GraphPad Prism version 8.00 for Windows. For Nmax comparison between hydrogel conditions, one-way ANOVA was performed. A p value lower than 0.05 was considered significant. Data is represented as mean ± SD.

Supporting Information

Supporting Information is available from the Wiley Online Library or from the author.

Acknowledgements

The authors would like to thank Dr. Susan Lindsay and Prof. Sue Barnett for providing the rat pups for the extraction of DRGs. Kind thanks to Dr. Manlio Tassieri for allowing use of the Rheometer and his support in analysis and interpreting the data. All the OPN and OCN images rendering in 3D and data analysis was possible with the help of Mr. Colin Loney by allowing access to the Imaris software. The authors acknowledge support via an EPSRC Programme Grant (EP/P001114/1).

Conflict of Interest

The authors declare no conflict of interest.

Author Contributions

O.D. formulated and developed the 3D LM/PEG hydrogels; she designed, performed or supervised all experiments and data analyses. M.A.G.O. performed experiments involving DRGs and analysed related data. G.C. performed bulk rheology experiments, and analysed bulk rheology data and contributed to the analysis of nanoindentation experiments. S.T. contributed to the development of hydrogels' formulation and characterisation (swelling, GFs release, LM distribution). A.R.N. contributed to developing the RNA extraction protocol in 3D hydrogels, image processing and the design of the paper figures. V.L.H. contributed to the image acquisition for the live/dead experiments. D.C.V. helped with DRG extraction protocols and DRG immunostaining. M.V. performed nanoindentation experiments and analysed related data using a custom-developed software (http://doi.org/10.5281/zenodo.4508646). C.G.G. contributed to experimental design and data interpretation. M.J.D. provided intellectual input to the project's conceptualisation and development. M.S.S. conceived, supervised and coordinated the project, and supplied the funds together with M.J.D., O.D., M.S.S, M.A.G.O. and G.C. wrote the paper and were involved in the editing process. S.T., A.R.N., M.V., C.G.G. and M.J.D. were involved in editing and proofreading of the manuscript.

Data Availability Statement

The data that support the findings of this study are openly available in University of Glasgow repository at https://doi.org/10.5525/gla.researchdata.1108.

Keywords

bone, growth factor, laminin, nerve, poly(ethylene) glycol

Received: November 28, 2020
Revised: February 14, 2021
Published online: March 21, 2021

[1] C. Frantz, K. M. Stewart, V. M. Weaver, *J. Cell Sci.* **2010**, *123*, 4195.
[2] C. S. Hughes, L. M. Postovit, G. A. Lajoie, *Proteomics* **2010**, *10*, 1886.
[3] E. A. Aisenbrey, W. L. Murphy, *Nat. Rev. Mater.* **2020**, *5*, 539.
[4] M. Salmerón-Sánchez, M. J. Dalby, *Chem. Commun.* **2016**, *52*, 13327.
[5] R. O. Hynes, *Science.* **2009**, *326*, 1216.
[6] A. Domogatskaya, S. Rodin, K. Tryggvason, *Annu. Rev. Cell Dev. Biol.* **2012**, *28*, 523.
[7] E. Hohenester, P. D. Yurchenco, E. Hohenester, P. D. Yurchenco, *Cell Adhes. Migr.* **2017**, *6918*, 56.
[8] D. Tsuruta, H. Kobayashi, H. Imanishi, K. Sugawara, M. Ishii, J. Jones, *Curr. Med. Chem.* **2008**, *15*, 1968.
[9] J. Ishihara, A. Ishihara, K. Fukunaga, K. Sasaki, M. J. V. White, P. S. Briquez, J. A. Hubbell, *Nat. Commun.* **2018**, *9*, 2163.
[10] P. Simon-Assmann, G. Orend, E. Mammadova-Bach, C. Spenlé, O. Lefebvre, *Int. J. Dev. Biol.* **2011**, *55*, 455.
[11] W. Wallquist, M. Patarroyo, S. Thams, T. Carlstedt, B. Stark, S. Cullheim, H. Hammarberg, *J. Comp. Neurol.* **2002**, *454*, 284.
[12] K. Garg, *Adv. Tissue Eng. Regener. Med.* **2017**, *2*, 194.
[13] I. Riederer, A. C. Bonomo, V. Mouly, W. Savino, *FEBS Lett.* **2015**, *589*, 3449.
[14] P. M. Gilbert, K. L. Havenstrite, K. E. G. Magnusson, A. Sacco, N. A. Leonardi, P. Kraft, N. K. Nguyen, S. Thrun, M. P. Lutolf, H. M. Blau, *Science* **2010**, *329*, 1078.
[15] F. Rohn, C. Kordes, M. Castoldi, S. Götze, G. Poschmann, K. Stühler, D. Herebian, A. S. Benk, F. Geiger, T. Zhang, J. P. Spatz, D. Häussinger, *Biomaterials* **2018**, *180*, 36.
[16] C. Ffrench-Constant, *Exp. Cell Res.* **1995**, *221*, 261.
[17] X. Ren, M. Zhao, B. Lash, M. M. Martino, Z. Julier, *Front. Bioeng. Biotechnol.* **2020**, *7*, 469.

[18] S. P. B. Teixeira, R. M. A. Domingues, M. Shevchuk, M. E. Gomes, N. A. Peppas, R. L. Reis, *Adv. Funct. Mater.* **2020**, *30*, 1909011.
[19] A. W. James, G. LaChaud, J. Shen, G. Asatrian, V. Nguyen, X. Zhang, K. Ting, C. Soo, *Tissue Eng., Part B* **2016**, *22*, 284.
[20] M. M. Martino, P. S. Briquez, K. Maruyama, J. A. Hubbell, *Adv. Drug Delivery Rev.* **2015**, *94*, 41.
[21] A. M. McCormick, N. A. Jarmusik, N. D. Leipzig, *Acta Biomater.* **2015**, *28*, 33.
[22] S. Noel, C. Fortier, F. Murschel, A. Belzil, G. Gaudet, M. Jolicoeur, G. De Crescenzo, *Acta Biomater.* **2016**, *37*, 69.
[23] M. M. Martino, P. S. Briquez, E. Güç, F. Tortelli, W. W. Kilarski, S. Metzger, J. J. Rice, G. A. Kuhn, R. MuÏller, M. A. Swartz, J. A. Hubbell, *Science* **2014**, *343*, 885.
[24] M. M. Martino, P. S. Briquez, A. Ranga, M. P. Lutolf, J. A. Hubbell, *Proc. Natl. Acad. Sci. U.S.A.* **2013**, *110*, 4563.
[25] K. M. Sawicka, M. Seeliger, T. Musaev, L. K. Macri, R. A. F. Clark, *Adv. Wound Care* **2015**, *4*, 469.
[26] J. C. Schense, J. A. Hubbell, *Bioconjugate Chem.* **1999**, *10*, 75.
[27] H. G. Schmoekel, F. E. Weber, J. C. Schense, K. W. Grätz, P. Schawalder, J. A. Hubbell, *Biotechnol. Bioeng.* **2005**, *89*, 253.
[28] V. Sacchi, R. Mittermayr, J. Hartinger, M. M. Martino, K. M. Lorentz, S. Wolbank, A. Hofmann, R. A. Largo, J. S. Marschall, E. Groppa, R. Gianni-Barrera, M. Ehrbar, J. A. Hubbell, H. Redl, A. Banfi, *Proc. Natl. Acad. Sci. U.S.A.* **2014**, *111*, 6952.
[29] R. Mittermayr, P. Slezak, N. Haffner, D. Smolen, J. Hartinger, A. Hofmann, J. Schense, D. Spazierer, J. Gampfer, A. Goppelt, H. Redl, *Acta Biomater.* **2016**, *29*, 11.
[30] E. Vardar, H. M. Larsson, S. Allazetta, E. M. Engelhardt, K. Pinnagoda, G. Vythilingam, J. A. Hubbell, M. P. Lutolf, P. Frey, *Acta Biomater.* **2018**, *67*, 156.
[31] M. M. Martino, F. Tortelli, M. Mochizuki, S. Traub, D. Ben-David, G. A. Kuhn, R. Müller, E. Livne, S. A. Eming, J. A. Hubbell, *Sci. Transl. Med.* **2011**, *3*, 100ra89.
[32] M. Mochizuki, E. Güç, A. J. Park, Z. Julier, P. S. Briquez, G. A. Kuhn, R. Müller, M. A. Swartz, J. A. Hubbell, M. M. Martino, *Nat. Biomed. Eng.* **2019**, *4*, 463.
[33] D. Barros, E. Conde-Sousa, A. M. Gonçalves, W. M. Han, A. J. García, I. F. Amaral, A. P. Pêgo, *Biomater. Sci.* **2019**, *7*, 5338.
[34] A. T. Francisco, P. Y. Hwang, C. G. Jeong, L. Jing, J. Chen, L. A. Setton, *Acta Biomater.* **2014**, *10*, 1102.
[35] A. T. Francisco, R. J. Mancino, R. D. Bowles, J. M. Brunger, D. M. Tainter, Y. Te Chen, W. J. Richardson, F. Guilak, L. A. Setton, *Biomaterials* **2013**, *34*, 7381.
[36] D. Barros, I. F. Amaral, A. P. Pêgo, *Biomacromolecules* **2020**, *21*, 276.
[37] D. Barros, P. Parreira, J. Furtado, F. Ferreira-da-Silva, E. Conde-Sousa, A. J. García, M. C. L. Martins, I. F. Amaral, A. P. Pêgo, *Biomaterials* **2019**, *192*, 601.
[38] J. Arulmoli, H. J. Wright, D. T. T. Phan, U. Sheth, R. A. Que, G. A. Botten, M. Keating, E. L. Botvinick, M. M. Pathak, T. I. Zarembinski, D. S. Yanni, O. V. Razorenova, C. C. W. Hughes, L. A. Flanagan, *Acta Biomater.* **2016**, *43*, 122.
[39] C. P. Addington, S. Dharmawaj, J. M. Heffernan, R. W. Sirianni, S. E. Stabenfeldt, *Matrix Biol.* **2017**, *60–61*, 206.
[40] C. P. Addington, J. M. Heffernan, C. S. Millar-Haskell, E. W. Tucker, R. W. Sirianni, S. E. Stabenfeldt, *Biomaterials* **2015**, *72*, 11.
[41] S. Trujillo, C. Gonzalez-Garcia, P. Rico, A. Reid, J. Windmill, M. J. Dalby, M. Salmeron-Sanchez, *Biomaterials* **2020**, *252*, 120104.
[42] S. Khetan, M. Guvendiren, W. R. Legant, D. M. Cohen, C. S. Chen, J. A. Burdick, *Nat. Mater.* **2013**, *12*, 458.
[43] Y. H. Tsou, J. Khoneisser, P. C. Huang, X. Xu, *Bioact. Mater.* **2016**, *1*, 39.
[44] S. A. Ferreira, M. S. Motwani, P. A. Faull, A. J. Seymour, T. T. L. Yu, M. Enayati, D. K. Taheem, C. Salzlechner, T. Haghighi, E. M. Kania, O. P. Oommen, T. Ahmed, S. Loaiza, K. Parzych, F. Dazzi, O. P. Varghese, F. Festy, A. E. Grigoriadis, H. W. Auner, A. P. Snijders, L. Bozec, E. Gentleman, *Nat. Commun.* **2018**, *9*, 5419.
[45] G. Ciccone, O. Dobre, G. M. Gibson, J. M. Rey, C. Gonzalez–Garcia, M. Vassalli, M. Salmeron–Sanchez, M. Tassieri, *Adv. Healthcare Mater.* **2020**, *9*, 2000517.
[46] O. Chaudhuri, *Biomater. Sci.* **2017**, *5*, 1480.
[47] C. F. Guimarães, L. Gasperini, A. P. Marques, R. L. Reis, *Nat. Rev. Mater.* **2020**, *5*, 351.
[48] A. M. Kloxin, C. J. Kloxin, C. N. Bowman, K. S. Anseth, *Adv. Mater.* **2010**, *22*, 3484.
[49] L. Marquardt, R. K. Willits, *J. Biomed. Mater. Res., Part A* **2011**, *98*, 1.
[50] X. Bai, M. Gao, S. Syed, J. Zhuang, X. Xu, X. Q. Zhang, *Bioact. Mater.* **2018**, *3*, 401.
[51] E. A. Phelps, N. O. Enemchukwu, V. F. Fiore, J. C. Sy, N. Murthy, T. A. Sulchek, T. H. Barker, A. J. García, *Adv. Mater.* **2012**, *24*, 64.
[52] C. Loebel, R. L. Mauck, J. A. Burdick, *Nat. Mater.* **2019**, *18*, 883.
[53] E. L. Qiao, S. Kumar, D. V. Schaffer, *Nat. Mater.* **2019**, *18*, 779.
[54] U. Blache, M. M. Stevens, E. Gentleman, *Nat. Biomed. Eng.* **2020**, *4*, 357.
[55] M. W. Tibbitt, K. S. Anseth, *Biotechnol. Bioeng.* **2009**, *103*, 655.
[56] D. Kesselman, O. Kossover, I. Mironi-Harpaz, D. Seliktar, *Acta Biomater.* **2013**, *9*, 7630.
[57] S. R. Caliari, J. A. Burdick, *Nat. Methods* **2016**, *13*, 405.
[58] H. Shih, C.-C. Lin, *Biomacromolecules* **2012**, *13*, 2003.
[59] K. Vats, G. Marsh, K. Harding, I. Zampetakis, R. E. Waugh, D. S. W. Benoit, *J. Biomed. Mater. Res., Part A* **2017**, *105*, 1112.
[60] N. Huebsch, P. R. Arany, A. S. Mao, D. Shvartsman, O. A. Ali, S. A. Bencherif, J. Rivera-Feliciano, D. J. Mooney, *Nat. Mater.* **2010**, *9*, 518.
[61] L. Yap, H. G. Tay, M. T. X. Nguyen, M. S. Tjin, K. Tryggvason, *Trends Cell Biol.* **2019**, *29*, 987.
[62] V. Llopis-Hernández, M. Cantini, C. González-García, Z. A. Cheng, J. Yang, P. M. Tsimbouri, A. J. García, M. J. Dalby, M. Salmerón-Sánchez, *Sci. Adv.* **2016**, *2*, e1600188.
[63] Z. A. Cheng, A. Alba-Perez, C. Gonzalez-Garcia, H. Donnelly, V. Llopis-Hernandez, V. Jayawarna, P. Childs, D. W. Shields, M. Cantini, L. Ruiz-Cantu, A. Reid, J. F. C. Windmill, E. S. Addison, S. Corr, W. G. Marshall, M. J. Dalby, M. Salmeron-Sanchez, *Adv. Sci.* **2018**, *6*, 1800361.
[64] M. H. Hettiaratchi, L. Krishnan, T. Rouse, C. Chou, T. C. McDevitt, R. E. Guldberg, *Sci. Adv.* **2020**, *6*, eaay1240.
[65] I. El Bialy, W. Jiskoot, M. Reza Nejadnik, *Pharm. Res.* **2017**, *34*, 1152.
[66] A. Cipitria, M. Salmeron-Sanchez, *Adv. Healthcare Mater.* **2017**, *6*, 1700052.
[67] H. S. Yang, W. G. La, Y. M. Cho, W. Shin, G. D. Yeo, B. S. Kim, *Exp. Mol. Med.* **2012**, *44*, 350.
[68] Medtronic, B, Important Med. Inf. 2004.
[69] W. Oripiriyakul, M. Tsimbouri, P. Childs, P. Campsie, J. Wells, M. M. Fernandez, K. Burgess, E. Tanner, M. Tassieri, D. Meek, M. Vassalli, M. Biggs, M. Salmeron-Sanchez, R. Oreffo, S. Reid, M. Dalby, *ACS Nano* **2020**, *14*, 10027.
[70] N. Ahimsadasan, A. Kumar, *Neuroanatomy, Dorsal Root Ganglion*, StatPearls Publishing, Treasure Island, FL **2018**.
[71] S. Plantman, M. Patarroyo, K. Fried, A. Domogatskaya, K. Tryggvason, H. Hammarberg, S. Cullheim, *Mol. Cell. Neurosci.* **2008**, *39*, 50.
[72] R. Li, D. Li, C. Wu, L. Ye, Y. Wu, Y. Yuan, S. Yang, L. Xie, Y. Mao, T. Jiang, Y. Li, J. Wang, H. Zhang, X. Li, J. Xiao, *Theranostics* **2020**, *10*, 1649.
[73] A. de Luca, P. di Summa, S. Lacour, W. Raffoul, *Neural Regener. Res.* **2014**, *9*, 1943.
[74] K. R. Jessen, R. Mirsky, *Front. Cell. Neurosci.* **2019**, *13*, 33.
[75] S. Carbonetto, M. Gruver, D. Turner, *Science.* **1982**, *216*, 897.
[76] A. M. Hopkins, L. De Laporte, F. Tortelli, E. Spedden, C. Staii, T. J. Atherton, J. A. Hubbell, D. L. Kaplan, *Adv. Funct. Mater.* **2013**, *23*, 5140.

[77] Z. Zhang, R. Yoo, M. Wells, T. P. Beebe, R. Biran, P. Tresco, *Biomaterials* **2005**, *26*, 47.
[78] A. Torres-Espín, D. Santos, F. González-Pérez, J. Del Valle, X. Navarro, *J. Neurosci. Methods* **2014**, *236*, 26.
[79] A. C. De Luca, A. Faroni, S. Downes, G. Terenghi, *Neurosci. Lett.* **2013**, *544*, 125.
[80] L. M. Marquardt, V. M. Doulames, A. T. Wang, K. Dubbin, R. A. Suhar, M. J. Kratochvil, Z. A. Medress, G. W. Plant, S. C. Heilshorn, *Sci. Adv.* **2020**, *6*, eaaz1039.
[81] S. J. Armstrong, M. Wiberg, G. Terenghi, P. J. Kingham, *Neurosci. Lett.* **2008**, *439*, 42.
[82] V. Iorio, L. D. Troughton, K. J. Hamill, *Adv. Wound Care* **2015**, *4*, 250.
[83] R. Carlsson, E. Engvall, A. Freeman, E. Ruoslahti, *Proc. Natl. Acad. Sci. U.S.A.* **1981**, *78*, 2403.
[84] M. Manthorpe, E. Engvall, E. Ruoslahti, F. M. Longo, G. E. Davis, S. Varon, *J. Cell Biol.* **1983**, *97*, 1882.
[85] A. Bartolozzi, F. Viti, S. De Stefano, F. Sbrana, L. Petecchia, P. Gavazzo, M. Vassalli, *J. Mech. Behav. Biomed. Mater.* **2020**, *103*, 103581.
[86] M. Vassalli, G. Ciccone, S. Ines, CellMechLab/nanoindentation: beta (Version v0.1.1). Zenodo, https://doi.org/10.5281/zenodo.4508646 (accessed: February 2021).
[87] T. Duanis-Assaf, Y. Razvag, M. Reches, *Anal. Methods* **2019**, *11*, 4709.